Mechanical Systems and Signal Processing, Volume 142, August 2020, Article number 106781
DOI: 10.1016/j.ymssp.2020.106781

An efficient electromagnetic and thermal modelling of eddy current pulsed thermography for quantitative evaluation of blade fatigue cracks in Heavy-duty Gas Turbines

Zongfei Tong[1], Shejuan Xie*[1], Haochen Liu[2], Cuixiang Pei[1], Cuixiang Pei[1], Yong Li[1], Zhenmao Chen*[1], Tetsuya Uchimoto[3], Toshiyuki Takagi[3]

[1]State Key Laboratory for Strength and Vibration of Mechanical Structures, Shaanxi Engineering Research Center of Nondestructive Testing and Structural Integrity Evaluation, Xi'an Jiaotong University, Xi'an 710049, China

[2] School of Aerospace, Transport and Manufacturing, Cranfield University, Bedfordshire MK43 0AL, U.K.

[3]Institute of Fluid Science, Tohoku University, Aoba-ku, Sendai, Miyagi 980-8577, Japan

The blade surface fatigue cracks often occur during service of Heavy-Duty Gas Turbines (HDGT) in high temperature, high rotational velocity and high frequency vibration environment. These fatigue cracks seriously threaten the safe operation of heavy-duty gas turbines, which would cause significant hazard or economic loss. The quantitative evaluation of blade surface fatigue cracks is extremely significant to HDGT. Eddy current pulsed thermography (ECPT) is an emerging non-destructive testing technology and show great potential for fatigue crack evaluation. This paper proposes a novel electromagnetic and thermal modelling of ECPT to achieve fast and effective

Published by Elsevier. This is the Author Accepted Manuscript issued with: Creative Commons Attribution Non-Commercial No Derivatives License (CC:BY:NC:ND 4.0).
The final published version (version of record) is available online at DOI:10.1016/j.ymssp.2020.106781. Please refer to any applicable publisher terms of use.

quantitative evaluation for surface fatigue cracks. First, the proposed numerical method calculates electromagnetic field using the reduced magnetic vector potential method in the frequency domain based on frequency series method. The thermal source is transformed to an equivalent and simple form according to the Energy equivalent method. Second, the temperature signals of ECPT are calculated through the time-domain iteration strategy with a relatively large time step. Then the ECPT experimental setup is established and the developed simulator is validated numerically and experimentally. The developed simulator is five times faster than the previous one and can be applied to eddy current thermography (ECT) with any kind of excitation waveforms. Finally, the depth of surface fatigue crack is quantitatively evaluated by means of the developed simulator, which is not only a promising simulation progress for ECPT, but also can be an effective tool embedded HDGT though-life maintenance.

***Index Terms*—Blade fatigue cracks, Heavy-duty gas turbines, Eddy current pulsed thermography, Quantitative evaluation, Fourier series method, Energy equivalent method**

1. INTRODUCTION

Heavy-duty gas turbine (see Fig. 1) blades serve in high temperature, high rotational velocity and high frequency vibration environments [1]. The severe serving conditions would increase the blades' material degradation and cause serious defects resulting in catastrophic failure and economic loss. It has been continuously reported that the fracture of blades is the chief crime to these failures. And, surface fatigue cracks are the main reason for the fracture

through the life of gas turbine [2]. In order to assure the structure safety and long-term reliability of gas turbine blade, the quantitative evaluation of the surface fatigue cracks of the GT blades is essential at early stage. Fortunately, the non-destructive testing and evaluation (NDT&E) techniques which have been improved decades, are very promising and suitable to this scenario.

In response to cracks, there are several conventional techniques such as ultrasonic testing, eddy current testing, acoustic emission. Recently, some emerging techniques have been developed in order to solve the mechanism issue in the industrial applications, like infrared thermography (IRT). IRT has many advantages including non-contact, greater inspection speed, higher resolution and sensitivity, detectability of inner defects due to heat conduction, and real-time measurements over a large detection area [3-5]. In addition, considering the large number of blades and short inspection time for the evaluation of the blade surface fatigue cracks, the inspection speed and detection accuracy are the factors that should be prioritized. Therefore, infrared thermography can be one great potential method to achieve the quantitative evaluation of blade fatigue cracks in heavy-duty gas turbine.

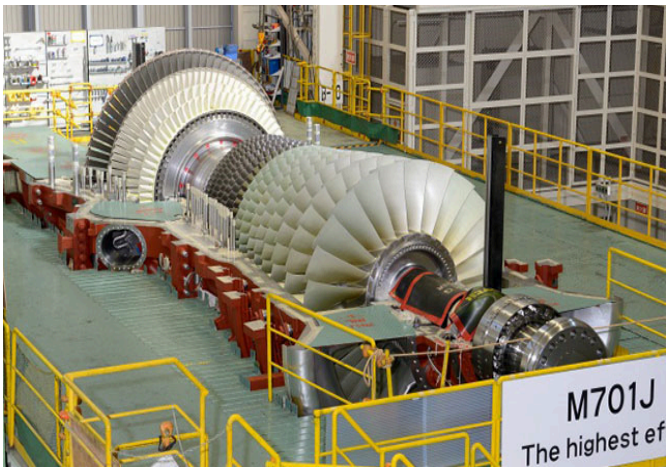


Fig. 1. Heavy-duty gas turbine

IRT is generally classified as "passive" and "active" thermography. Active IRT employs external excitation source such as flash lamps [6], eddy current [7], laser thermography [8], optical lock-in thermography [9], microwave excitation [10] or sonic excitation [11] to generate heat in the component within inspection. The eddy current stimulated thermography (ECT) has many potential advantages over other excitation techniques for IRT: the surface condition of the component under inspection has less effect on the ECT than optical excitation IRT; it can easily induce high temperature rise and thermal pulse in conductive materials especially metals; the material under inspection could not be damaged since the heating is limited to dozens of centigrade; and, for near-surface defects, direct interaction with eddy currents can improve detectability [12].

Eddy current stimulated heating mode for thermography could be applied in terms of pulsed thermography (ECPT) [13-14], step thermography, lock-in thermography [15], and pulsed phase thermography [16]. As a popular transient electromagnetic-thermal NDT, ECPT involves the application of a high frequency electromagnetic excitation (typically 50-500 KHz) to induce eddy currents flowing inside the material under inspection, at a large current for a short period [17]. The typical configuration of the ECPT system is shown in Fig. 2. The excitation signal generated by the induction heating system is a high-frequency current pulse continuing for a few milliseconds. It is then driven by the transmitter coil above the conductor to induce eddy current and heat the material with resistive heat. In addition, circulating cooling water through the coil is performed to eliminate thermal radiation by the brass coil. Three-dimensional heat diffusion leads the flow from a high to low temperature area, and then reduces the contrast until the heat is balanced in the material [18-19]. A defect in the conductive material (see Fig. 3) will disturb the distribution of eddy current and

the process of thermal diffusion [20]. Therefore, by capturing the transient thermal response of the resultant surface, the material defects can be detected and evaluated [21].

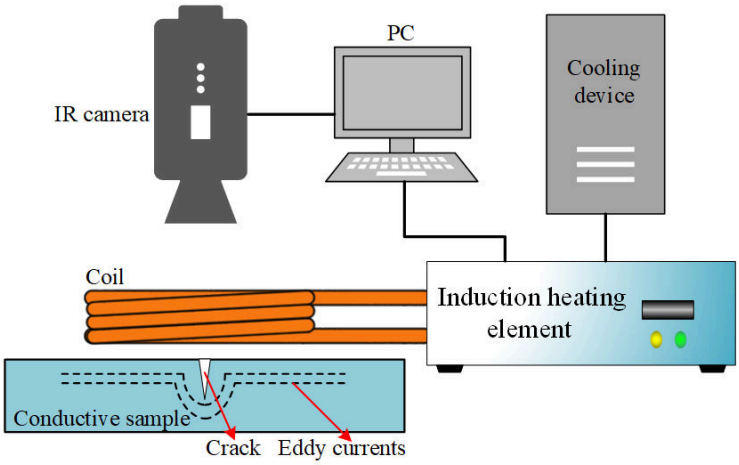


Fig. 2. Basic configuration of an ECPT system

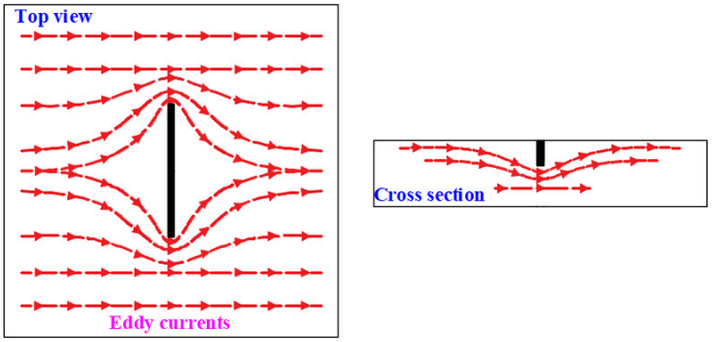


Fig. 3. Schematic of theoretical eddy current distribution for crack

The ECPT can achieve high speed inspection compared to conventional thermography methods. Besides, lots of time is required to clean the blades in conventional inspection techniques to assure enough energy introduction and high-quality data capturing. The ECPT also does not require any contact with the inspected target of turbine blades. For the quantitative evaluation of surface fatigue cracks, the length and width of crack can be quantitatively inspected through infrared image sequences [4]. However, the crack depth is

difficult to determine only from infrared image sequences directly, which is the main factor leading to the blade fracture. In this paper, an efficient and fast numerical method of ECPT signal prediction is proposed and developed to help to evaluate crack depth quantitatively.

The excitation signal of ECPT is a small period of high-frequency current (typically 50-500 KHz), which increases the difficulty of simulation of ECPT signals efficiently and accurately. In response to numerical simulation of ECPT signal, most previous research calculated the ECPT signals in the time domain. Abidin et al. simulated the transient thermal distribution for angular slots, via time-stepping 3D finite element analysis (FEA) [7]. Liu et al. used ANSYS software to solve the coupled electromagnetic and temperature field equations in the time domain and the frequency of the excitation current is 1.6 kHz [22]. He et al. used COMSOL Multiphysics to simulate the ECPT signals of wall thinning defect and inner defect in steel under transmission mode and reflection mode, and he also simulated the signals of crack with corrosion on the basis of ECPT [23-24]. These works provide great contributions for the development of ECPT inspection method in the NDT field. However, simulating ECPT signals in the time domain is rather time-consuming and requires high computing resources. Some researches proposed several numerical methods for induction heating problem [25-26], but these methods are just valid for harmonic excitation, although the excitation waveforms of ECPT are not limited to harmonics.

In previous work, a numerical method for ECPT based on FEM-BEM method and energy equivalent principle is proposed and validated [27]. However, the coefficient matrices of electromagnetic field of the proposed method is not sparse due to the incorporation of BEM, which leads to relatively long calculation time and more calculation resource. In addition, a fast simulator will be very helpful for both the model-based defect sizing using inverse

problems and the optimization of the excitation probe in the development process of ECPT method. According to the above state-of-arts, this paper proposes a numerical method to calculate ECPT signals efficiently in the frequency domain combined with the time domain based on the Fourier series method [28] and the Energy equivalent method [29]. Different from the previous work, this method employs edge elements in the process of simulation of electromagnetic field and the application of reduced magnetic vector potential method avoids generating complex meshes in the air region [30]. As a mature method abbreviated as "Ar" from its developer and many researches, the reduced magnetic vector potential method will be denoted as "Ar" method below, unless specified otherwise.

The rest of the paper is organized as follows: First, the principle of the proposed electromagnetic numerical method using Ar method based on the Fourier series method is introduced in Section 2. Then the temperature field simulation method based on the Energy equivalent method is presented in Section 3. The proposed ECPT numerical method is validated in Section 4 through comparison with the commercial COMSOL Multiphysics software. An ECPT experiment for 304 stainless steel plates with slot defect are carried out in Section 5 under reflection mode by means of configuring the camera and the probe on the same side of the specimen. The quantitative evaluation of surface fatigue cracks using proposed method is presented in Section 6. Finally, conclusions are outlined in Section 7.

2. NUMERICAL METHOD FOR ELECTROMAGNETIC FIELD

The proposed numerical method for ECPT is applied to solve the coupled electromagnetic and temperature field. As the frequency band of the ECPT excitation typically locates in a small period of high-frequency current (typically 50-500 KHz), the simulation of ECPT

signals in the time domain is time-consuming and requires very high computing resources. Fortunately, the response signals of electromagnetic field could be calculated efficiently and rapidly in the frequency domain. The excitation current could be treated as a summation of a series of sinusoidal waves with different harmonic frequencies and corresponding amplitudes [28]. Additionally, the material properties can be considered as independent from temperature because the temperature rise within the specimen is very low. Therefore, the response signal of the electromagnetic field is also composed of the sinusoidal waves of the frequencies that appeared in the driving current. Based on these considerations, the electromagnetic response signal of the ECPT could be acquired through calculating the response signal of sinusoidal excitation current of a single frequency initially. Then by the summation of the response signal of every harmonic frequency, the target results are obtained. The strategy for calculating the electromagnetic response signal of ECPT is called the Fourier series method.

2.1 Calculation of the response signal of the single-frequency sinusoidal excitation

The reduced magnetic vector potential method (Ar method) is employed to simulate the response signal of single-frequency sinusoidal excitation current using edge elements in this study. In the Ar method, the whole analysis region is divided into two parts, which are shown in Fig. 4. V_t is the part that includes the conductive or ferromagnetic material in which the standard magnetic potential A is selected. V_r is the remainder of the analysis region in which the reduced magnetic potential $\boldsymbol{A}_r$ is used. When the edge elements are used, a gauge

condition of $\varphi = 0$ can be applied [30]. Therefore, the governing equations of the Ar method can be written as:

$$\nabla \times \frac{1}{\mu} \nabla \times \boldsymbol{A} + \sigma \frac{\partial \boldsymbol{A}}{\partial t} = 0 \ , \quad \text{in } V_t \qquad (1)$$

$$\nabla \times \frac{1}{\mu_0} \nabla \times \boldsymbol{A}_r = 0 \ , \quad \text{in } V_r \qquad (2)$$

where μ_0 is the permeability of the air, μ is the permeability of the conductor, σ is the conductivity of the conductor, and $\boldsymbol{A}$ and $\boldsymbol{A}_r$ are the standard and reduced magnetic potentials, respectively ($\boldsymbol{A} = \boldsymbol{A}_r + \boldsymbol{A}_s$. $\boldsymbol{A}_r$ is the reduced magnetic vector potential which is generated only by eddy current in the conductor, and $\boldsymbol{A}_s$ is the magnetic vector potential which is generated only by source current).

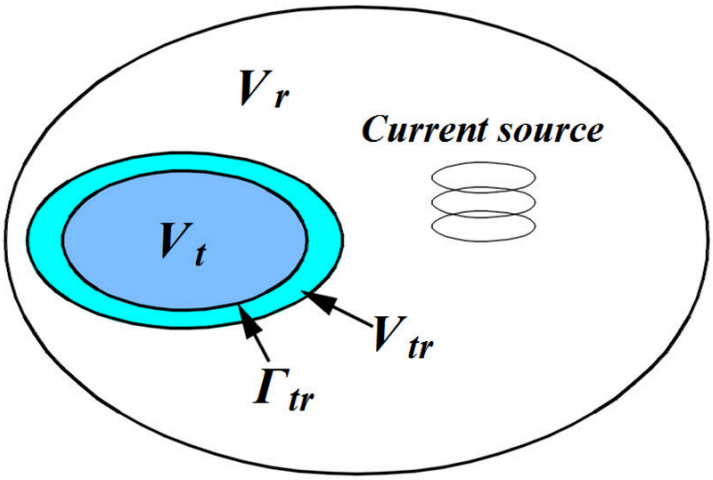


Fig. 4. Computational model in the reduced magnetic vector potential method

According to the boundary condition, for the joining of these two regions, the continuity of the magnetic flux density and magnetic field could be represented by:

$$\boldsymbol{n} \times \boldsymbol{A} = \boldsymbol{n} \times (\boldsymbol{A}_r + \boldsymbol{A}_s), \quad \text{on } \Gamma_{\text{tr}} \qquad (3)$$

$$\boldsymbol{n}\times\frac{1}{\mu}(\nabla\times\boldsymbol{A})=\boldsymbol{n}\times(\frac{1}{\mu_0}\nabla\times\boldsymbol{A}_r+\boldsymbol{H}_s),\quad \text{on } \Gamma_{\text{tr}} \qquad (4)$$

where $\boldsymbol{n}$ is a unit normal vector on Γ_{tr}, and $\boldsymbol{A}_s$ and $\boldsymbol{H}_s$ are the magnetic vector potential and magnetic field generated by the current source located in V_r, respectively. Equations (1) and (2) are coupled via these conditions. $\boldsymbol{A}_s$ and $\boldsymbol{H}_s$ can be calculated using Biot-Savart's law independently of the finite elements:

$$\boldsymbol{H}_s=\frac{1}{4\pi}\int_{V_c}\boldsymbol{J}_s\times\nabla\frac{1}{R}dV \qquad (5)$$

$$\boldsymbol{A}_s=\frac{\mu_0}{4\pi}\int_{V_c}\frac{\boldsymbol{J}_s}{R}dV \quad (6)$$

where V_c is the region of the current source, $\boldsymbol{J}_s$ is the current density in the excitation coil and R is the distance from the point of the current source $\boldsymbol{J}_s$ to the point of the field of $\boldsymbol{A}_s(\boldsymbol{H}_s)$.

The governing equations, (1) and (2), and the boundary conditions, (3) and (4) could be discredited through Galerkin's FEM discretization strategy as shown in (7).

$$[K]\{\boldsymbol{A}\}+[C]\left\{\frac{\partial\boldsymbol{A}}{\partial t}\right\}=\{M\}I(t) \qquad (7)$$

where $I(t)$ denotes the time function of excitation current source, $[K]$, $[C]$, $[M]$ are coefficient matrices of FEM equations.

Moreover, (8) can be obtained using complex approximation in case that the excitation current is a single-frequency sinusoidal wave. Namely, setting $\partial\boldsymbol{A}/\partial t=j\omega\boldsymbol{A}$, where ω is the angular frequency of the excitation signal:

$$[K]\{\boldsymbol{A}\} + j\omega[C]\{\boldsymbol{A}\} = \{M\} I \quad (8)$$

The developed code of Ar method is used to calculate the electromagnetic response signal of the single-frequency sinusoidal excitation current.

2.2 Principle of the Fourier series method

I(t) in (7) is a time dependent function, and it can be expressed as (9) through a discrete Fourier transformation,

$$I(t) = \sum_{n=1}^{N} \widetilde{F}_n e^{j\omega_n t} \quad (9)$$

where ω_n is the angular frequency of the sinusoidal excitation and $\widetilde{F}_n$ denotes the amplitude coefficient. Since the (7) is a linear differential equation, its solution has the form:

$$\{\boldsymbol{A}(\boldsymbol{t})\} = \sum_{n=1}^{N} \{\widetilde{\boldsymbol{A}_n}\} e^{j\omega_n t} \quad (10)$$

Substituting the (10) into the (7), the (7) can be expressed as the following form:

$$\sum_{n=1}^{N} \left([K] + j\omega_n [C]\right) \{\widetilde{\boldsymbol{A}_n}\} e^{j\omega_n t} = \sum_{n=1}^{N} \{M\} \widetilde{F}_n e^{j\omega_n t} \quad (11)$$

Equation (11) is equivalent to:

$$\left([K] + j\omega_n [C]\right) \{\widetilde{\boldsymbol{A}_n}\} = \{M\} \widetilde{F}_n \quad (12)$$

Each equation of the equation system (12) has the same form as (8). Therefore, the potential response A_{n0} due to a unit current source can be obtained using the method described in section 2.1. Once each A_{n0} has been calculated, the final solution of (7) could

be calculated by superimposing the response signal of each frequency, which is shown in (13).

$$\left\{\boldsymbol{A}(t)\right\} = \sum_{n=1}^{N} \widetilde{F}_n \left\{\widetilde{\boldsymbol{A}_{n0}}\right\} e^{j\omega_n t} \quad (13)$$

Equation (13) shows that, the response magnetic vector potential $\boldsymbol{A}$ is composed of components of the same harmonic frequencies as the excitation current of ECPT. The response signal can be obtained by summing the response signals of the single-frequency sinusoidal excitation currents with the proper weight coefficients.

The eddy current density $\boldsymbol{J}$, which is induced in the conductor by the excitation coil, could also be calculated through superimposing the eddy currents due to single-frequency sinusoidal excitation. Namely,

$$\left\{\boldsymbol{J}(t)\right\} = -\sigma\left\{\frac{\partial \boldsymbol{A}(t)}{\partial t}\right\} = \sum_{n=1}^{N} \widetilde{F}_n \left(-j\omega_n \sigma \left\{\widetilde{\boldsymbol{A}_{n0}}\right\}\right) e^{j\omega_n t} \quad (14)$$

Equation (14) could be rewritten as the following equation,

$$\left\{\boldsymbol{J}(t)\right\} = \sum_{n=1}^{N} \widetilde{F}_n \left(\widetilde{\boldsymbol{J}_{n0}}\right) e^{j\omega_n t} \quad (15)$$

where J_{n0} is the eddy current due to a single-frequency and unit amplitude excitation.

Based on the equations described above, the eddy current density which is the thermal source of the temperature field could be calculated from a sum of the response signals of the sinusoidal excitation currents with the proper weight coefficients.

3. NUMERICAL STRATEGY FOR TEMPERATURE FIELD

In terms of the thermal analysis, the constant material properties can be adopted because the temperature rise of ECPT within the specimen is not more than 100 or 150 ℃. As the heating saturation is 0.2 s, the heat transfer through convection and radiation is neglected. The heat conduction is the main type of heat transfer. Therefore, the governing equation of the temperature field could be written as follows:

$$\rho C_p \frac{\partial T}{\partial t} = k\nabla^T \nabla T + Q, \quad \text{in } \Omega \quad (16)$$

where T, ρ, C_p, and k are the temperature, the density, the specific heat, and the thermal conductivity, respectively. Q denotes the thermal source. Ω is a bounded domain representing all the conductive media.

The adiabatic boundary condition is adopted on the boundary $\partial\Omega$, which could be expressed as follows:

$$\frac{\partial T}{\partial n} = 0, \quad \text{on } \partial\Omega \quad (17)$$

where n is a unit normal vector on $\partial\Omega$.

To calculate of ECPT response, Q in (16) represents the power losses through the Joule effect. The mean power over one time step Δt of the source current could be expressed as the following:

$$Q = \frac{1}{\sigma \Delta t} \int_0^{\Delta t} \boldsymbol{J}^2(t) dt \quad (18)$$

Considering the high frequency of the eddy current density $J(\mathrm{t})$ due to the high frequency of the excitation current, it would be time-consuming in case that temperature field

is calculated through the time step iteration in the time domain directly. One of the conventional processing methods is to locally linearize the thermal source based on the Energy equivalent method [29]. The excitation of high frequency in the calculation of the temperature field can be transformed to an equivalent simple form according to the energy equivalent method as shown in Fig. 5. In each time step Δt, the sinusoidal thermal excitation Q of high frequency is transformed to a linear excitation $\widetilde{Q}$. The energy of the excitations before and after transformation keeps the same, i.e., the area S1 enclosed by the original thermal excitation curve and the x coordinate axis equals to the area S2 enclosed by the transformed thermal excitation curve and the x coordinate axis. The $\widetilde{Q}$ is presented in (19).

$$\widetilde{Q}(\mathrm{t}) = \frac{\int_{t-\Delta t/2}^{t+\Delta t/2} Q(\mathrm{t})\,\mathrm{dt}}{\Delta t} \qquad (19)$$

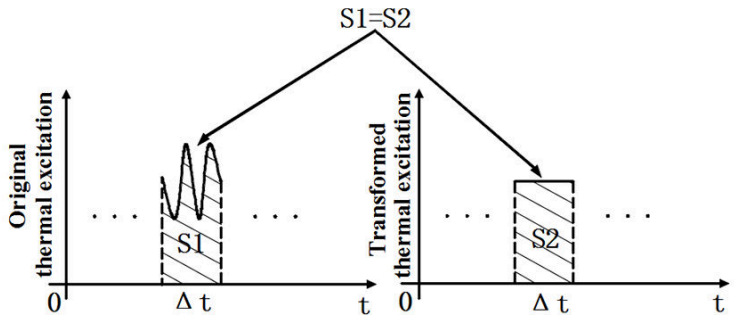


Fig. 5. Equivalent principle of the energy equivalent method

Based on the principle of energy equivalent method described above, equation (16) is equivalent to:

$$\rho C_p \frac{\partial T}{\partial t} = k\nabla^T \nabla T + \widetilde{Q}\,, \quad \text{in } \Omega \qquad (20)$$

Equation (20) is solved through Crank-Nicolson time iterative integration method in the time domain. This method is based on the central difference method which is the average of the forward Euler method and the backward Euler method. The governing equation could be expressed as the following form:

$$\left[\left[K\right](1-\zeta)+\frac{\left[C\right]}{\Delta t}\right]\left\{T\right\}_{t+\Delta t}=\{\widetilde{Q}\}_{t+\Delta t}+\left[\frac{\left[C\right]}{\Delta t}-\zeta\left[K\right]\right]\left\{T\right\}_{t} \qquad (21)$$

where $\left[K\right]$, $\left[C\right]$, and $\left[\widetilde{Q}\right]$ are the coefficients matrix of the thermal conductivity, the specific heat and the heat flux density, respectively. ζ has a value range of 0-1, which determines the stability and accuracy of convergence.

Iterations of the (21) are performed until the maximum variation of degrees of freedom between two successive iterations becomes less than prescribed thresholds. In our case, these thresholds are defined at the beginning of the iteration process using the coefficient $\varepsilon=10^{-3}$ which could satisfy the numerical accuracy.

4. THE NUMERICAL VALIDATION OF THE PROPOSED METHOD

A numerical code for calculating the response signals of ECPT is developed based on the theory described in section 2 and 3. In order to validate the reliability of the proposed method and the developed simulator, the temperature distribution of a square flawless copper plate stimulating by a circle excitation coil were calculated using the developed code and the COMSOL Multiphysics, respectively. The geometrical data and physical parameters used for this problem are displayed in table 1. Notice that these data do not take into account the

temperature dependence due to that the temperature rise within the specimen is very low. Three-dimensional meshes have been employed in this numerical method, and the numerical solutions obtained by the developed simulator were compared with the results of COMSOL Multiphysics. The geometry and the mesh used for this simulation are shown in Fig. 6 and Fig. 7, respectively. To avoid edge effect, the size of the plate is much larger than the size of excitation coil.

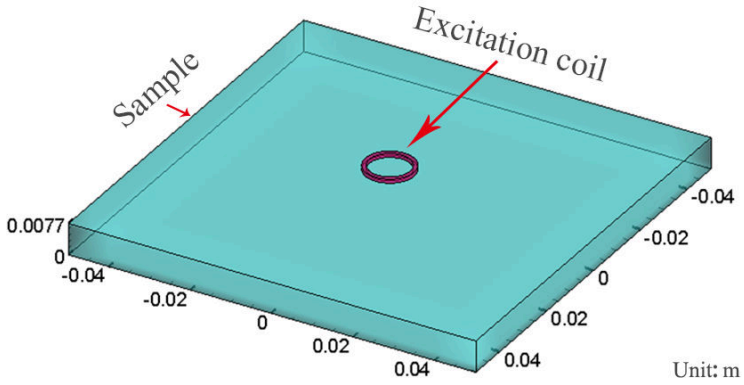


Fig. 6. The numerical models of excitation coil and plate

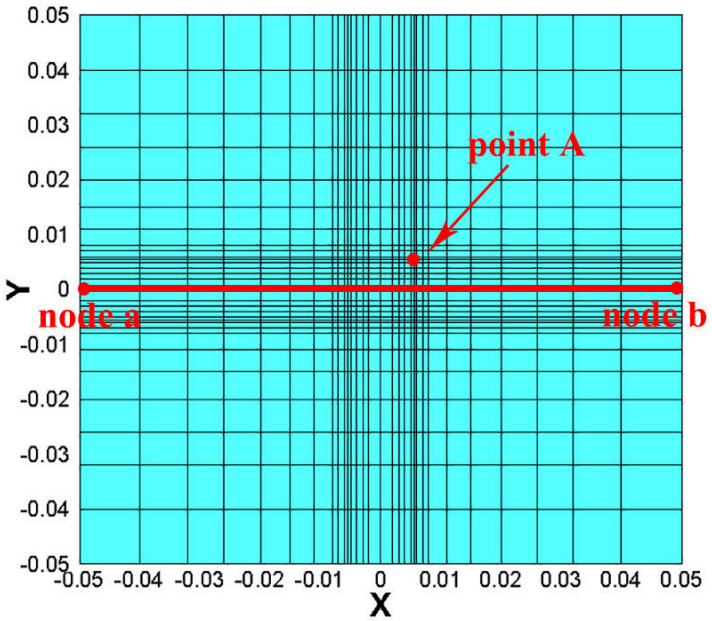


Fig. 7. The mesh of two slices from the numerical model

The heating time and cooling time of excitation current both set at 0.2 s. The frequency of excitation current in the simulation is set at 50 Hz which is rather lower than the frequency of experiments, so that the amplitude of excitation current is set at 38000 A which is higher than the excitation current of experiments to ensure the numerical accuracy. The setting of low frequency of excitation current is just to make the process of the simulation time-saving through the commercial Multiphysics software which calculates the response signals in the time domain. That is to say, the setting of high frequency of excitation current such as (50-500) kHz which is usually employed in the experiment will make the signal prediction significantly time-consuming using COMSOL software. For example, if the excitation frequency of 325 kHz (employed in the experiment of this study) is used in the simulation using COMSOL software, to guarantee the numerical accuracy, around 1 million calculation steps need to be adopted during the heating stage of 0.2s in the time calculus method, which will need an intolerable long time consuming. To avoid the above case, a relative low excitation frequency of 50 Hz is employed in the COMSOL simulation process. However, according to the induction heating theory, such a low frequency of 50 Hz will rapidly decrease the heating effect, may leading to around only 1×10^{-6} degrees Celsius temperature rise if still combination with 380A excitation current. 1×10^{-6} degrees Celsius temperature rise is really difficult to ensure its simulation accuracy. Hence, a 38000 A excitation current is adopted in the simulation, just in order to increase the induction heating effect, and then give us a platform to validate the numerical accuracy of the developed ECPT signal simulator through comparing its results with the commercial COMSOL results.

Table 1

Geometrical data and physical parameters

Items	Specification
Specimen size	Square flawless plate Side length: 100 mm; Thickness: 7.7 mm;
Liftoff distance	0.5 mm
Excitation coil size	Outer radius: 6.0 mm Inner radius: 5.0 mm Height: 1.0 mm Number of coil turns: 1 turn
Heat transfer coefficient	Cu: 8700 kg/m^3, 385 J/(kg • K), 400 W/(m • K);
Electromagnetic parameters	Cu: Electrical conductivity: 5.998×10^7 S/m Magnetic relative permeability: 1.0

To validate the reliability of the simulation of temperature field of the proposed method as well as the developed simulator, firstly, the temperature profiles of point A (0.004, 0.004, 0.0077) (see Fig. 7) at different time steps from 0 to 0.4 s is provided in Fig. 8. Fig 8 shows that the profiles of heating stage at point A from COMSOL is oscillating. The temperature results at point A from 0.12 s to 0.16 s are displayed in Fig. 9 to explain the oscillation of temperature. The temperature rising from point L to point M (see Fig. 9) indicates that the heat generated by the eddy current is more than the heat diffusion. On the contrary, the heat generated by the eddy current is less than the heat diffusion from point M to point N. On the other hand, since the energy equivalent strategy is employed during the small time interval (Δt) in the proposed simulation method, we can see that the heat generated by the heat source is always more than the heat diffusion, which cause the temperature is monotonically increasing along the time slide. The relative error of the maximum temperature from 0 to 0.4 s of two methods is 0.32%. The comparison between the temperature variation of developed simulator and the temperature envelope curves of COMSOL is presented in Fig. 10.

At the beginning of heating stage, the temperature results approach the upper envelope curve of COMSOL since that the equivalent heat source is higher than that of the real case. In the rest of the heating stage, the temperature results of developed simulator are between the upper and lower envelope curves of COMSOL, which is corresponding to the principle of energy equivalent method. Finally, the temperature along the line between node a (-0.05, 0, 0.0077) and node b (0.05, 0, 0.0077) (see Fig. 7) at the time = 0.18 s is presented in Fig. 11. The relative error of the maximum temperature along the line at the time = 0.18 s is 1.23%. Therefore, we can see that the results of temperature of the developed simulator have good agreements with the solutions of COMSOL. The computation efficiency of two methods in same calculation environment are listed in table II. The speed of proposed numerical method is 10 times faster than the time iteration strategy and 5 times than the previous research [27]

Table 2

Computation efficiency

Items	COMSOL	Simulator of previous research	Developed simulator
Elements	31375 (Air, coil and metal)	8192 (Only metal)	40572 (Air and metal)
CPU	4	1	1
Elapsed time	10779 s	5400 s	815 s

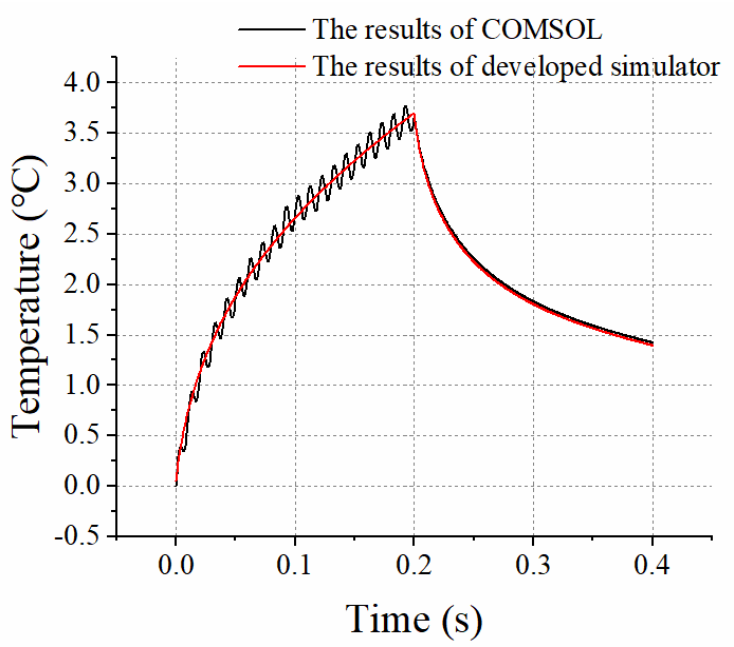


Fig. 8. Temperature profiles at point A

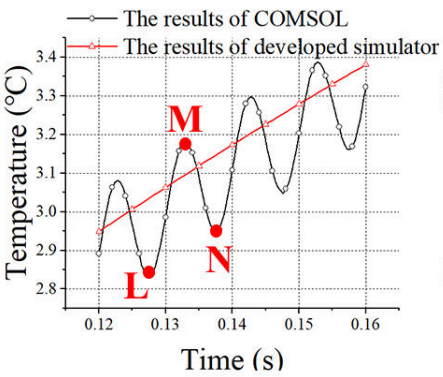


Fig. 9. Temperature profiles at point A from 0.12 s to 0.16 s

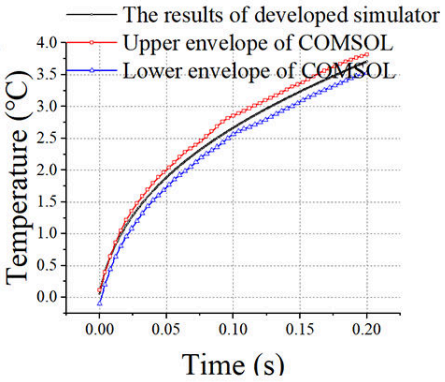


Fig. 10. Temperature profiles at point A in heating stage

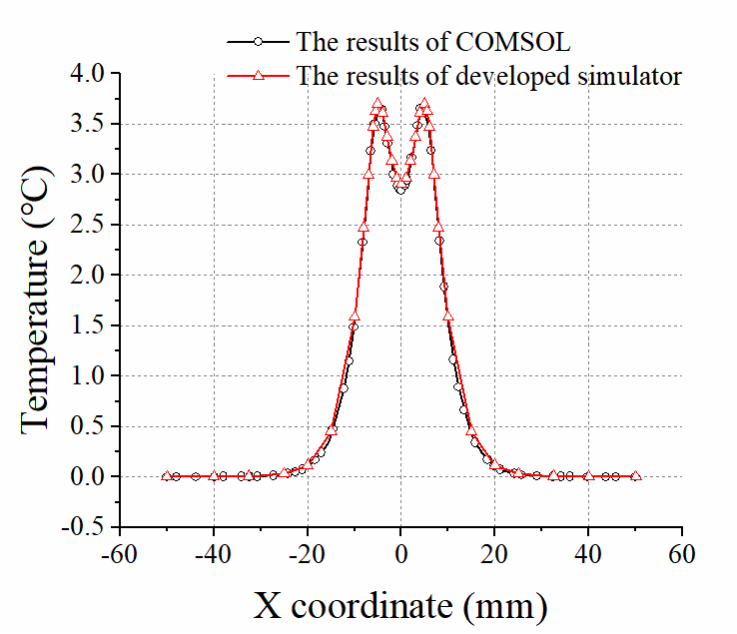


Fig. 11. Temperature profiles between node a and node b at time = 0.18 s

5. THE EXPERIMENTAL VALIDATION OF THE PROPOSED METHOD

In this section, experiments are carried out to verify the developed simulation method. The ECPT system used in this study is introduced firstly. Then, the ECPT experiments and numerical simulation of 304 stainless steel flawless plates are carried out under reflection mode by means of configuring the camera and the probe on the same side of the specimen. Finally, the ECPT experimental signals and the results of numerical simulation of the plates with slot defect are presented.

5.1 ECPT system configuration

The ECPT experimental system is established which is shown in Fig. 12. The excitation sub-system is based around a commercial induction heating system, the Easyheat 224 from

AMBRELL Precision Induction Heating. The Easyheat has a maximum excitation power of 2.4 kW, a maximum current of 400 Arms and an excitation frequency range of 150 kHz – 400 kHz (384.8 Arms and 325 kHz are used during this study). The Easyheat 224 needs around 50 ms to reach maximum power which has been validated in the experiments. Water cooling of excitation coil is implemented to counteract direct heating of the coil.

An Flir camera is carried out in ECPT system which has a sensitivity of < 20 mK and a maximum full frame rate of 60 Hz. The Fig. 14 shows the excitation coil used in the tests which is made of 6.00 mm diameter hollow copper tube with high conductivity and the diameter of the coil is 100.0 mm. In this study, the frame rate is 60 Hz, and 4 s videos are recorded in the experiments where the heating stage is 0.2 s.

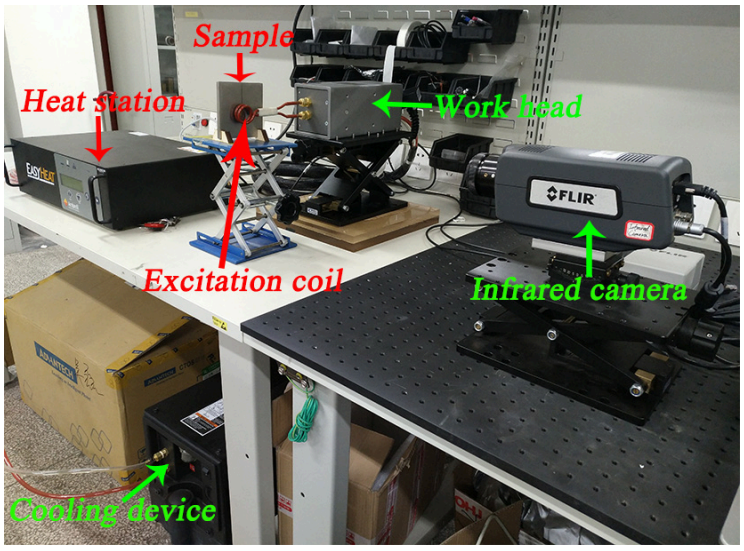


Fig. 12. Experiment setup

5.2 The ECPT experiments and numerical simulation of 304 stainless steel plate with a slot crack

The turbine blade is shown in Fig. 13, which is made of nickel-based alloy. As a result of that the conductivity of nickel-based alloy (1.0 MS/m) is similar to that of 304 stainless steel (1.3 MS/m) and both of them are non-ferromagnetic material, the 304 stainless steel is used to approximate nickel-based alloy. Additionally, the curvature of the detected area is relatively small in most part of the entire blade. Therefore, the plate model is adopted to approximate the inspected area. It is worth noting that the proposed method is also effective for the complex numerical model, and only the calculation scale is larger.



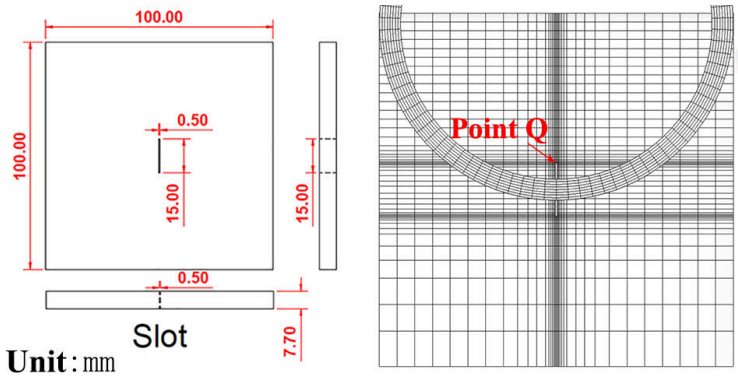
Fig. 13. Heavy-duty gas turbine blade

In order to validate the reliability of developed simulator for the defective sample, in this section, one 304 stainless steel plate with a slot crack is employed whose size is shown in Fig. 14(a). The relative position between the plate specimen and the excitation coil is shown in Fig. 15, where the liftoff distance is 0.5 mm and the size of the excitation coil is also the same as in previous section 5.1.

The numerical model of 304 stainless steel plate with a slot crack is presented in Fig. 14(b) which consists 62422 elements. It can be seen from Fig. 16 that the temperature near the crack tips is higher than the surrounding area. For the purpose of reducing the randomness

of the experiment results, the experiments were conducted four times at different times and the mean of repetitions are adopted to prove the experimental robustness.

The temperature variation (the experimental temperature minus ambient temperature) from 0 to 4 s at the crack tip (Point Q) is extracted from the image sequences. Fig. 17 gives error bar of the temperature difference of four experiment results and simulation results at point Q (see Fig. 16) at different time steps from 0 to 4 s. The results of temperature for 304 stainless steel plate with a slot crack of the developed simulator have good agreements with the results of experiments in the heating stage. In the cooling stage, although the temperature of developed simulator drops faster than the average temperature of four experiments, the numerical results have good coherence in the scope of errors. In the environment of Intel(R) Core(TM) i5-6500 CPU (also RAMs and operating system), the simulation elapsed time is 1739 s.



(a) (b)

Fig. 14. (a) The sizes of 304 stainless steel plates with a slot crack, (b)The numerical model for 304 stainless steel plate with a slot crack

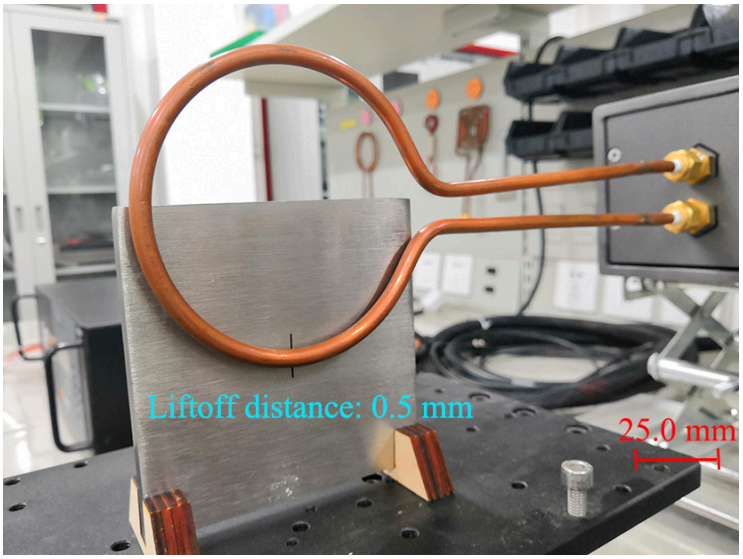
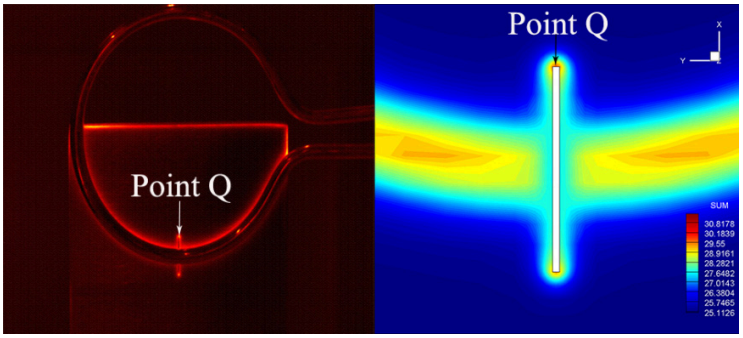


Fig. 15. The experiment configuration of ECPT applied to a plate with a slot crack



(a) (b)

Fig. 16. (a) The thermal image after 0.18 s of heating for 304 stainless steel plate with a slot crack, (b) The corresponding temperature results of simulation

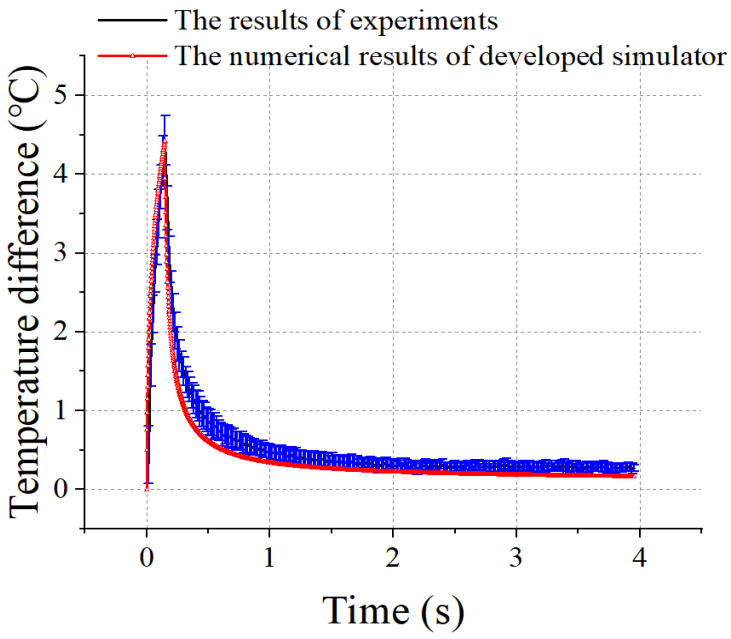


Fig. 17. Transient temperature profiles of the point Q.

6. THE QUANTITATIVE EVALUATION OF SURFACE FATIGUE CRACKS

To quantitative evaluation of surface cracks, the characterization of crack depth is the crucial and difficult. The length and width of crack can be quantitatively inspected through infrared image sequences, however, the crack depth cannot be directly determined only from the infrared images. Moreover, the surface crack depth is the main factor leading to turbine blade fracture. In section 5, it has been proved that the developed simulator can predict ECPT signals efficiently and reliably. Therefore, the proposed method is applied to quantitatively evaluate the depth of the surface crack in this section.

The size of the numerical model is the same as the previous section (see fig.14(a)) except that the crack depth is different, which is shown in Fig. 18. The variance depths of the surface cracks are set as 2.7, 1.7, 1.2, 0.7, and 0.2 mm, respectively. The transient temperature

profiles at the tip of all different cracks are presented in Fig. 19, which indicate that the depth is sensitive to temperature rise, peaks and decay profiles. It demonstrates that the proposed method is promising to quantitatively evaluated the crack depth.

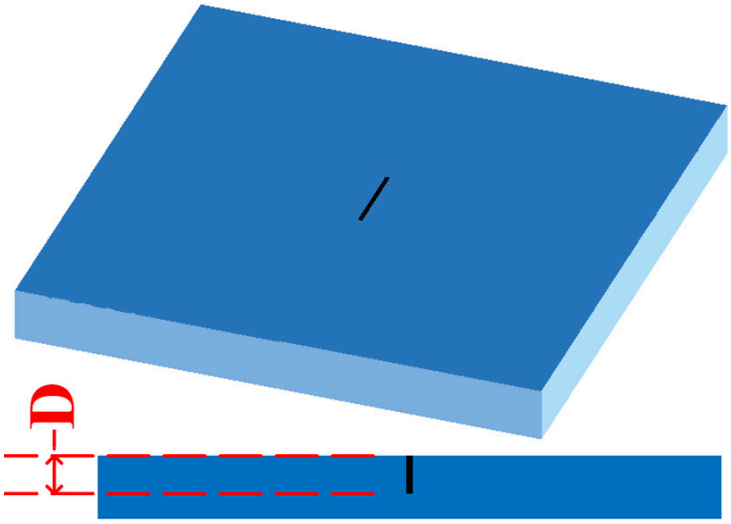


Fig. 18. Numerical model with a surface crack

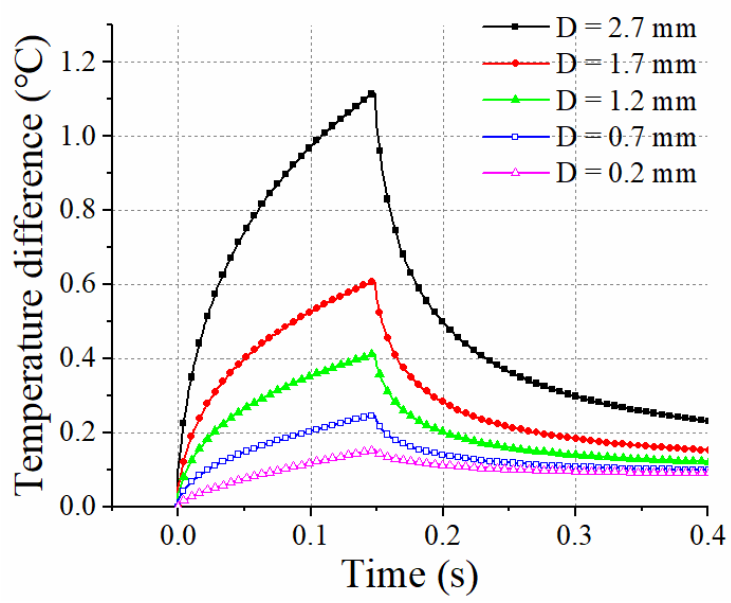


Fig. 19. The temperature difference of surface cracks at different depths

7. CONCLUSIONS

In order to achieve quantitative evaluation of blade fatigue cracks in heavy-duty gas turbines, this paper proposes a numerical method for signal prediction of ECPT based on the Fourier series method and the energy equivalent method. The developed simulator calculates electromagnetic field in the frequency domain using Fourier series method and simulates temperature field in the time domain through energy equivalent method. The contributions show the following:

1) The proposed numerical strategy speeds up the numerical simulation of ECPT signals in a huge step and can be applied to eddy current thermography with different excitation waveforms. For simulation of electromagnetic field, the reduced magnetic vector potential method using edge element is employed, which accelerate the calculation speed compared with FEM-BEM method in previous work. The Fourier series method accelerates the simulation of electromagnetic field faster than time iteration strategy, reducing the effect of high frequency excitation current on numerical simulation speed. In addition, the application of energy equivalent method in temperature field calculation process eliminates the influence of high frequency thermal source on numerical simulation speed, which can employ relatively large time step in the time domain.
2) Through the ECPT experiments, the length and width of crack can be quantitatively inspected through thermal images easily, then the surface crack depth is quantitatively evaluated though the developed numerical simulator efficiently and reliably. The proposed method and corresponding simulator have great potential to help to ensure the safety of heavy-duty gas turbines blades.

For the quantitative evaluation of surface/near surface cracks with regular dimension, the crack depth at the tip can be accurately quantified. In the future, for the complicated shaped cracks, the quantitative analysis of three dimensions of crack size including crack depth should be assisted by furtherly progressed inversion algorithms for higher accuracy in complex defect scenario based on ECPT signals.

ACKNOWLEDGMENT

The authors would like to thank the National Science Foundation of China (51877163, 51577139).

REFERENCES

[1] B. Salehnasab, E. Hajjari, S.A. Mortazavi, Failure Assessment of the First Stage Blade of a Gas Turbine Engine, Transactions of the Indian Institute of Metals, 70 (2017) 2103-2110.
[2] S. Lecheb, T. Djedid, A. Chellil, A. Nour, M. Cherigui, H. Kebir, Fatigue crack initiation and vibration prediction life of turbine blade, 2013, pp. 1-6.
[3] H. Liu, C. Pei, S. Xie, Y. Li, Y. Zhao, Z. Chen, Inversion Technique for Quantitative Infrared Thermography Evaluation of Delamination Defects in Multilayered Structures, IEEE Transactions on Industrial Informatics, (2019) 1-1.
[4] G. Zenzinger, J. Bamberg, M. Dumm, P. Nutz, Crack Detection Using EddyTherm, AIP Conference Proceedings, 760 (2017) 1646.
[5] L. Haochen, S. Xie, C. Pei, J. Qiu, Y. Li, Z. Chen, Development of a Fast Numerical Simulator for Infrared Thermography Testing Signals of Delamination Defect in a Multilayered Plate, IEEE Transactions on Industrial Informatics, 14 (2018) 5544-5552.
[6] N.P. Avdelidis, B.C. Hawtin, D.P. Almond, Transient thermography in the assessment of defects of aircraft composites, Ndt & E International, 36 (2003) 433-439.
[7] I.Z. Abidin, G.Y. Tian, J. Wilson, S.X. Yang, D. Almond, Quantitative evaluation of angular defects by pulsed eddy current thermography, Ndt & E International, 43 (2010) 537-546.
[8] J. Qiu, C. Pei, H. Liu, Z. Chen, K. Demachi, Remote inspection of surface cracks in metallic structures with fiber-guided laser array spots thermography, Ndt & E International, 92 (2017) 213-220.
[9] Z.C. Marguerite, Quantitative Analyse von Defekten in kohlefaserverstärktem Kunststoff mittels optisch angeregter Lockin Thermographie, 2009.
[10] D. Bates, G. Smith, D. Lu, J. Hewitt, Rapid thermal non-destructive testing of aircraft components, Compos Part B-Eng, 31 (2000) 175-185.
[11] M. Morbidini, P. Cawley, The detectability of cracks using sonic IR, J Appl Phys, 105 (2009) 1-9.
[12] S. Pickering, D. Almond, Matched excitation energy comparison of the pulse and lock-in thermography NDE techniques, Ndt & E International, 41 (2008) 501-509.

[13] L. Cheng, B. Gao, G.Y. Tian, W.L. Woo, G. Berthiau, Impact Damage Detection and Identification Using Eddy Current Pulsed Thermography Through Integration of PCA and ICA, Ieee Sens J, 14 (2014) 1655-1663.
[14] B. Gao, L.B. Bai, W.L. Woo, G.Y. Tian, Y.H. Cheng, Automatic Defect Identification of Eddy Current Pulsed Thermography Using Single Channel Blind Source Separation, Ieee T Instrum Meas, 63 (2014) 913-922.
[15] G. Riegert, T. Zweschper, G. Busse, Eddy-current lockin-thermography: Method and its potential, J Phys Iv, 125 (2005) 587-591.
[16] Y.Z. He, M.C. Pan, G.Y. Tian, D.X. Chen, Y. Tang, H. Zhang, Eddy current pulsed phase thermography for subsurface defect quantitatively evaluation, Appl Phys Lett, 103 (2013) 054103-052120.
[17] G.G. Yen, K.-C. Lin, Wavelet packet feature extraction for vibration monitoring, IEEE Transactions on Industrial Electronics, 47 (2000) 650-667.
[18] G.Y. Tian, Y.L. Gao, K.J. Li, Y.Z. Wang, B. Gao, Y.Z. He, Eddy Current Pulsed Thermography with Different Excitation Configurations for Metallic Material and Defect Characterization, Sensors-Basel, 16 (2016) 843.
[19] Y.L. Gao, G.Y. Tian, K.J. Li, J. Ji, P. Wang, H.T. Wang, Multiple cracks detection and visualization using magnetic flux leakage and eddy current pulsed thermography, Sensor Actuat a-Phys, 234 (2015) 269-281.
[20] M. Pan, Y. He, G. Tian, D. Chen, F. Luo, Defect characterisation using pulsed eddy current thermography under transmission mode and NDT applications, Ndt & E International, 52 (2012) 28-36.
[21] B. Gao, Y. He, W. Lok Woo, G. Yun Tian, J. Liu, Y. Hu, Multidimensional Tensor-Based Inductive Thermography With Multiple Physical Fields for Offshore Wind Turbine Gear Inspection, IEEE Transactions on Industrial Electronics, 63 (2016) 6305-6315.
[22] G.F. Liu, G.H. Li, Numerical simulation of defect inspection using electromagnetically stimulated thermography, Journal of Shanghai Jiaotong University(Science), 16 (2011) 262-265.
[23] Y.Z. He, M.C. Pan, F.L. Luo, Defect characterisation based on heat diffusion using induction thermography testing, Rev Sci Instrum, 83 (2012) 433-439.
[24] Y. He, G. Tian, L. Cheng, H. Zhang, P. Jackson, Corrosion Characterisation under Coating Using Pulsed Eddy Current Thermography, 50th Annual Conference of the British Institute of Non-Destructive Testing 2011 (NDT 2011) :, Telford, (-uk), 2011, pp. 259-269.
[25] Y. Masuda, T. Tsukada, M. Hozawa, N. Imaishi, N. Ohnishi, Numerical simulation of heat transfer in floating zone single crystal growth process with radio frequency induction heating, International Journal of Heat & Mass Transfer, 39 (1996) 3035–3043.
[26] S. Teniou, M. Meribout, K. Al-Wahedi, A. Al-Durra, E. Al-Hosani, A Near-Infrared-Based Magnetic Induction Tomography Solution to Improve the Image Reconstruction Accuracy in Opaque Environments, IEEE Transactions on Magnetics, 49 (2013) 1361-1366.
[27] Z. Tong., S. Xie., X. Li., C. Pei., Z. Chen., Y. He., Efficient numerical simulation of eddy current pulsed thermography NDT signals based on FEM-BEM Method and Energy Equivalent Principle, Infrared Physics & Technology, 101 (2019) 138-145.
[28] S. Xie, Z. Chen, T. Takagi, T. Uchimoto, Efficient Numerical Solver for Simulation of Pulsed Eddy-Current Testing Signals, IEEE Transactions on Magnetics, 47 (2011) 4582-4591.
[29] S. Patankar, Numerical Heat Transfer and Fluid Flow, McGraw Hill Book Company, New York, 1980.
[30] T. Takagi, Haoyu Huang, H. Fukutomi, Junji Tani, Numerical evaluation of correlation between crack size and eddy current testing signal by a very fast simulator, IEEE Transactions on Magnetics, 34 (1998) 2581-2584.



https://dspace.org/

An efficient electromagnetic and thermal modelling of eddy current pulsed thermography for quantitative evaluation of blade fatigue cracks in heavy-duty gas turbines

Tong, Zongfei; Xie, Shejuan; Liu, Haochen; Zhang, Weixu; Pei, Cuixiang ...

2020-03-19
Elsevier
https://doi.org/10.1016/j.ymssp.2020.106781
Tong Z, Xie S, Liu H, et al., (2020) An efficient electromagnetic and thermal modelling of eddy current pulsed thermography for quantitative evaluation of blade fatigue cracks in heavy-duty gas turbines. Mechanical Systems and Signal Processing, Volume 142, August 2020, Article number 106781

Downloaded from a DSpace repository. https://dspace.org/